

# Mass distributions marginalized over per-event errors

D. Martínez Santos<sup>a</sup>, F. Dupertuis<sup>b</sup>

<sup>a</sup>*NIKHEF and VU University Amsterdam, Amsterdam, The Netherlands*

<sup>b</sup>*Ecole Polytechnique Fédérale de Lausanne (EPFL), Lausanne, Switzerland*

---

## Abstract

We present generalizations of the Crystal Ball function to describe mass peaks in which the per-event mass resolution is unknown and marginalized over. The presented probability density functions are tested using a series of toy MC samples generated with Pythia and smeared with different amounts of multiple scattering and for different detector resolutions.

*Keywords:* statistics, invariant mass peaks

---

## 1. Introduction

A very common probability density function (*p.d.f.*) used to fit the mass peak of a resonance in experimental particle physics is the so-called Crystal Ball (CB) function [1–3]:

$$p(m) \propto \begin{cases} e^{-\frac{1}{2}\left(\frac{m-\mu}{\sigma}\right)^2} & , \text{ if } \frac{m-\mu}{\sigma} > -a \\ A \left(B - \frac{m-\mu}{\sigma}\right)^n & , \text{ otherwise} \end{cases} \quad (1)$$

where  $m$  is the free variable (the measured mass),  $\mu$  is the most probable value (the resonance mass),  $\sigma$  the resolution,  $a$  is called the transition point and  $n$  the power-law exponent.  $A$  and  $B$  are calculated by imposing the continuity of the function and its derivative at the transition point  $a$ . This function consists of a Gaussian core, that models the detector resolution, with a tail on the left-hand side that parametrizes the effect of photon radiation by the final state particles in the decay. In data analysis, one may deal with events which have different uncertainties on the measured mass, therefore distorting the core of the Crystal

21 Ball, which will not be a Gaussian any more. This is sometimes modelled by the  
 22 sum of two or three Crystal Ball functions, which is the equivalent of assuming  
 23 that the per-event uncertainty is a sum of two or three delta functions. However,  
 24 per-event uncertainties are usually continuous functions very different from a  
 25 sum of a small number of deltas. One way of dealing with per-event uncertainties  
 26 that follow a certain distribution, is to either make a *p.d.f.* conditional on the  
 27 per-event uncertainty (if its distribution is known) or to perform the analysis  
 28 in bins of the quantities that affect the per-event uncertainties (for example,  
 29 particle momenta) and combine them afterwards. However, those procedures  
 30 can significantly complicate the analysis, and in some cases one may prefer to  
 31 simply marginalize over the mass error and have a *p.d.f.* that describes the final  
 32 mass peak, as:

$$p(m) \propto \int_0^\infty \frac{1}{\sqrt{v}} e^{-\frac{1}{2v}(m-\mu)^2} \rho(v) dv \quad (2)$$

33 where  $v$  is the variance and  $\rho(v)$  the prior density of the variance.

34 In this paper, we will define some extensions of the Crystal Ball distribution  
 35 for different assumptions on  $\rho(v)$ . We will fit the proposed mass models to  
 36  $J/\psi \rightarrow \mu^+ \mu^-$  toy MC samples where we can modify the relative importance of  
 37 multiple scattering (MS) and detector spatial resolution (hereafter SR). Section  
 38 2 describes the generation of the toy MC samples. Section 3 defines an extension  
 39 of the CB using a hyperbolic distribution core. Sections 4 and 5 generalize the  
 40 function defined in Sect. 3. Section 6 gives a brief discussion of the meaning  
 41 of the fit parameters. Section 7 discusses other effects on the invariant mass  
 42 line-shape that are not directly related to resolution. Conclusions are drawn in  
 43 Sect. 8.

## 44 2. Simulation of $J/\psi \rightarrow \mu^+ \mu^-$ decays

45 We generate  $J/\psi$  events at  $\sqrt{s} = 8$  TeV using the `main17.cc` script of  
 46 `Pythia8.176` [4]. The  $J/\psi$ 's are then isotropically decayed into two muons. No

47 photons are added, as the radiative tail of the mass distribution should be well  
 48 accounted by the Crystal Ball tail.

The generated muon momenta are smeared with a Gaussian resolution which has a momentum dependence:

$$\frac{\sigma(p)}{p} = a + bp \quad (3)$$

49 where  $a$  mimics the multiple scattering (MS) and  $b$  mimics the effect of the hit  
 50 resolution. We take as typical values  $a = 3 \times 10^{-3}$  and  $b = 2 \times 10^{-5} \text{ GeV}^{-1}c$   
 51 inspired by [5], although we will vary them for different tests.

### 52 **3. Hyperbolic resolution model**

53 A very flexible function that describes asymmetric unimodal *p.d.f.*'s defined  
 54 above a certain threshold (i.e, like per-event error distributions usually look  
 55 like, see for example Fig. 6 in [6]) is the so-called Amoroso distribution [7] (see  
 56 Fig. 3). If we consider the Amoroso distribution as a potential implementation  
 57 for  $\rho(v)$ , then the corresponding core of the invariant mass *p.d.f.* will be the  
 58 following:

$$\Phi(m) \propto \int_0^\infty \frac{1}{\sqrt{v}} e^{-\frac{1}{2v}(m-\mu)^2} \left(\frac{v-v_0}{\theta}\right)^{\alpha\beta-1} e^{-\left(\frac{v-v_0}{\theta}\right)^\beta} dv \quad (4)$$

59 Unfortunately, the above integral cannot be solved analytically. It would  
 60 require a numerical implementation of the core and its derivative. This would  
 61 make the matching with the radiative tail difficult. Evaluating (4) numerically  
 62 for different values of Amoroso parameters, we find log-densities that exhibit an  
 63 hyperbolic profile. Based on that observation, we define a possible core:

$$c(x) \propto e^{-b\sqrt{1+(m-\mu)^2/\delta^2}} \quad (5)$$

i.e,  $c(x)$  is the symmetric limit of the hyperbolic distribution. It can also be rewritten in such way that the mass resolution  $\sigma$  appears explicitly, as it will be discussed in Sect. 4. Adding a CB-like tail to (5), we obtain the following

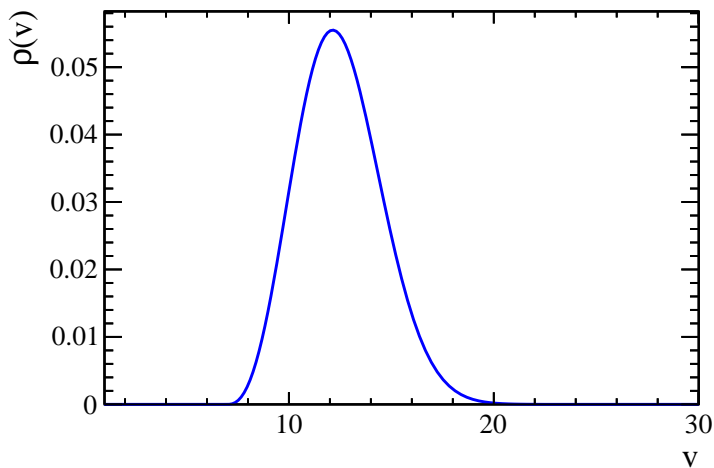


Figure 1: Example of the Amoroso distribution for a hypothetical variance  $v$ . The parameters used are  $\theta = 5$ ,  $\alpha = 1.5$ ,  $\mu = 7$ , and  $\beta = 2.3$ .

*p.d.f.:*

$$A(m, \mu, b, \delta, a, n) \propto \begin{cases} e^{-b\sqrt{1+(m-\mu)^2/\delta^2}} & , \text{ if } \frac{m-\mu}{\delta} \geq -a \\ e^{-b\sqrt{1+a^2}} \left( \frac{n\sqrt{1+a^2}}{ba(n\sqrt{1+a^2}/(ba)-a-(m-\mu)/\delta)} \right)^n & , \text{ otherwise} \end{cases} \quad (6)$$

hereafter referred to as the *Apollonios* distribution, currently being used for cross-checks in data analysis of the LHCb experiment. The core (5) can be obtained analytically for a variance prior density:

$$\rho(v, b, \delta) \propto e^{-(b^2 v/\delta^2 + \delta^2/v)} \quad (7)$$

64 We fit the mass peak for  $J/\psi \rightarrow \mu^+ \mu^-$  decays satisfying  $p_T^{J/\psi} \in [0, 14] \text{ GeV}/c$ ,  
65  $\theta^\mu \in [20, 300] \text{ mrad}$ ,  $p^\mu > 6 \text{ GeV}/c$ ,  $p_T^\mu > 0.5 \text{ GeV}/c$  (which mimics LHCb-like  
66 conditions) to the *Apollonios* distribution, and find a very good agreement as  
67 can be seen in Fig. 3.

68 Now, the good agreement between this model and the MC toys used for  
69 testing can be broken without too much effort. For example, we now repeat  
70 the exercise releasing all kinematic and acceptance cuts, and switching off the

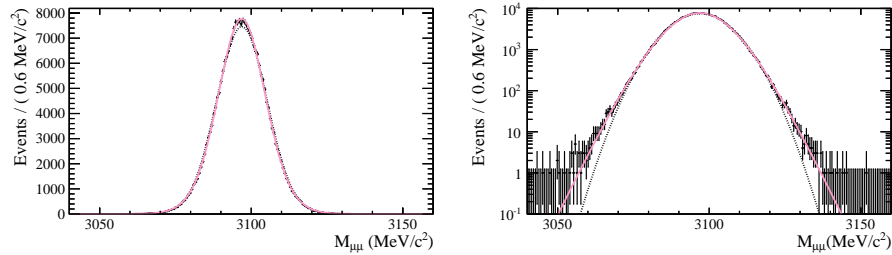


Figure 2: Fit of the invariant mass distribution of a  $J/\psi \rightarrow \mu^+\mu^-$  generated sample with  $p_T^{J/\psi} \in [0, 14]$  GeV/c,  $\theta_\mu \in [20, 300]$  mrad,  $p^\mu > 6$  GeV/c and  $p_T^\mu > 0.5$  GeV/c. The pink line corresponds to the fit to a hyperbolic distribution. The dashed black line corresponds to the fit to a Gaussian. Left: linear scale. Right: Logarithmic scale.

71 MS term. These changes modify the distribution and fit results are shown in  
 72 Fig. 3, where we see that (5) cannot fit the generated data. However, it is also  
 73 interesting to note that, even in this extreme case, (5) can do a good job in a  
 74 region of about two standard deviations around the peak.

#### 75 4. Generalized Hyperbolic resolution model

The core of (5) is a limit case of the generalized hyperbolic distribution [8]:

$$G(m, \mu, \lambda, \alpha, \beta, \delta) = ((m - \mu)^2 + \delta^2)^{\frac{1}{2}\lambda - \frac{1}{4}} e^{\beta(m - \mu)} K_{\lambda - \frac{1}{2}} \left( \alpha \sqrt{(m - \mu)^2 + \delta^2} \right) \quad (8)$$

76 where  $K_\lambda$  are the cylindrical harmonics or special Bessel functions of third kind.  
 77 In principle,  $\beta^2$  is constrained to be smaller than  $\alpha^2$ . In practice that condition  
 78 can be ignored if the fitting range is finite, but one has to be careful that if  $\beta^2 >$   
 79  $\alpha^2$  one of the tails will start rising at some point. The generalized hyperbolic  
 80 distribution also has an important limit case, the *Student's-t* distribution, as  
 81 indicated in Table 1.

82 The *p.d.f.* in (8) can also be obtained by marginalizing over a variance  
 83 density<sup>1</sup>:

<sup>1</sup>The parameter  $\beta$  is related to a variance-dependency of the Gaussian mean, and not to

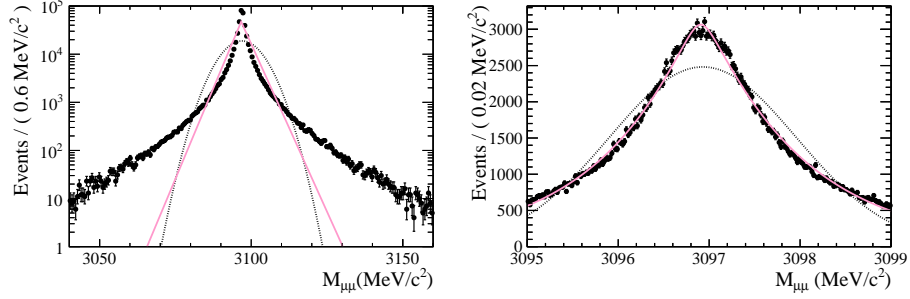


Figure 3: Fit of the invariant mass distribution of a  $J/\psi \rightarrow \mu^+\mu^-$  generated sample without any phase space restriction and without the multiple scattering term in the momentum resolution. The pink line corresponds to the fit to an hyperbolic distribution. The dashed black line corresponds to the fit to a Gaussian. Left: Fit in the full mass range. Right: Fit in a region of about two standard deviations around the mean.

Table 1: Limit cases of the generalized hyperbolic distribution

Distributions	$G(m, \mu, \lambda, \alpha, \beta, \delta)$
Hyperbolic	$\lambda = 1, \alpha\delta = b$
Symmetric hyperbolic	$\lambda = 1, \beta = 0, \alpha\delta = b$
Student's t	$\lambda = -\frac{\nu}{2}, \alpha = 0, \beta = 0, \delta = \sqrt{\nu}$
Non-standardized Student's t	$\lambda = -\frac{\nu}{2}, \alpha = 0, \beta = 0$

$$\rho(v, \lambda, \alpha, \delta) \propto v^{\lambda-1} e^{-[\alpha^2 v + \delta^2/v]} \quad (9)$$

84 The distribution (9) is the generalized inverse Gaussian distribution and de-  
 85 scribes very well the density we find for  $\sigma_{\mu\mu}^2$ , for the example in Fig. 3. This is  
 86 shown in Fig. 4, together with the good agreement between the simulated data  
 87 and the generalized hyperbolic distribution. We find that (9) fits well the mass  
 88 variance distribution for all the generated  $J/\psi \rightarrow \mu^+ \mu^-$  samples that we have  
 89 tested, although one needs to add an overall offset to the per-event error, i.e, to  
 90 change  $v$  by  $v - v_0$  in (9). The effect of an overall displacement of the per-event  
 91 error distribution is further discussed in Sect. 5.

The following re-parametrization  $\{\alpha; \delta\} \rightarrow \{\sigma; \zeta\}$ :

$$\zeta = \alpha\delta \quad (10)$$

$$\sigma^2 = \delta^2 \frac{K_{\lambda+1}(\zeta)}{\zeta K_{\lambda}(\zeta)} = \delta^2 A_{\lambda}^{-2}(\zeta) \quad (11)$$

92 is more suitable for fitting purposes as it allows us to specify the rms ( $\sigma$ ) of  
 93 the distribution in the symmetric case ( $\beta = 0$ ) as an explicit parameter.  $A_{\lambda}^2 =$   
 94  $\frac{\zeta K_{\lambda}(\zeta)}{K_{\lambda+1}(\zeta)}$  is introduced for further convenience. In that parametrization:

$$G(m, \mu, \sigma, \lambda, \zeta, \beta) \propto ((m - \mu)^2 + A_{\lambda}^2(\zeta)\sigma^2)^{\frac{1}{2}\lambda - \frac{1}{4}} e^{\beta(m - \mu)} K_{\lambda - \frac{1}{2}} \left( \zeta \sqrt{1 + \left(\frac{m - \mu}{A_{\lambda}(\zeta)\sigma}\right)^2} \right) \quad (12)$$

95 Figure 4 shows  $G(m, \mu, \sigma, \lambda, \zeta, \beta)$  for different values of  $\zeta$  and  $\lambda$ .

Using (12) as the core of a CB-like function, we define:

$$I(m, \mu, \sigma, \lambda, \zeta, \beta, a, n) \propto \begin{cases} ((m - \mu)^2 + A_{\lambda}^2(\zeta)\sigma^2)^{\frac{1}{2}\lambda - \frac{1}{4}} e^{\beta(m - \mu)} K_{\lambda - \frac{1}{2}} \left( \zeta \sqrt{1 + \left(\frac{m - \mu}{A_{\lambda}(\zeta)\sigma}\right)^2} \right) & , \text{ if } \frac{m - \mu}{\sigma} > -a \\ \frac{G(\mu - a\sigma, \mu, \sigma, \lambda, \zeta, \beta)}{\left(1 - m / \left(n \frac{G(\mu - a\sigma, \mu, \sigma, \lambda, \zeta, \beta)}{G(\mu - a\sigma, \mu, \sigma, \lambda, \zeta, \beta)} - a\sigma\right)\right)^n} & , \text{ otherwise} \end{cases} \quad (13)$$

---

the per event variance distribution. For the purpose of this paper  $\beta$  can be considered zero.

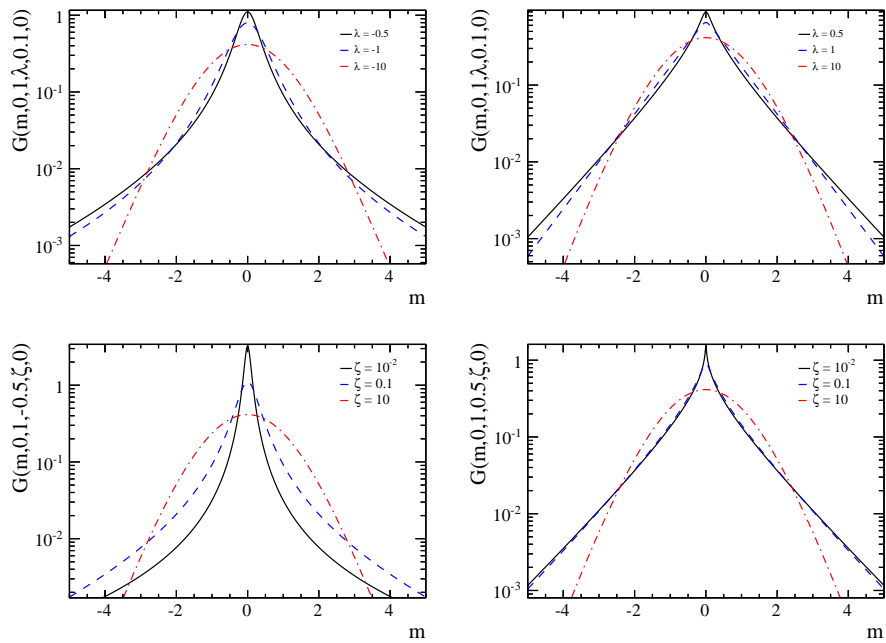


Figure 4:  $G(m, \mu, \sigma, \lambda, \zeta, \beta)$  is plotted for standard values of  $\mu, \sigma, \beta$  and different values of  $\zeta$  and  $\lambda$ . *Top:*  $\zeta$  is fixed to 0.1 and  $\lambda$  is varied. *Bottom:*  $\lambda$  is fixed to -0.5 for the *left* plot and 0.5 for the *right* plot and  $\zeta$  is varied.

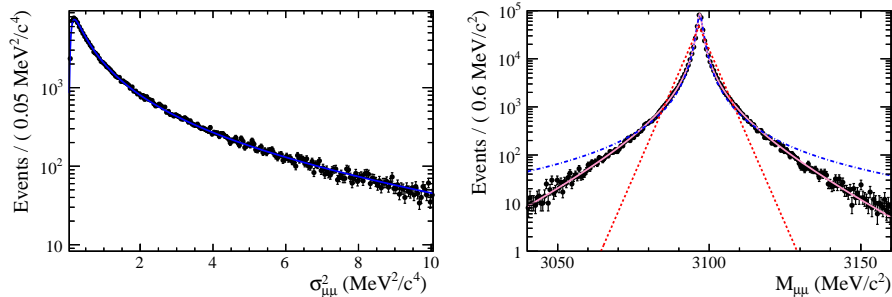


Figure 5: Left: Per-event mass error squared fitted to (9) in a  $J/\psi \rightarrow \mu^+\mu^-$  sample generated without MS. Right: Fit to the mass distribution on the same sample. The pink solid line shows the generalized hyperbolic. The dot-dashed blue line the *Student's-t* case, and the dashed red line the hyperbolic distribution.

96 hereafter referred to as *Hypatia* distribution, where  $G'$  is the derivative of the  
 97  $G$  defined in (8).

98 The generalized hyperbolic core can describe most of the examples that were  
 99 generated (see Fig. 4, right), but can also be broken with high statistic samples  
 100 if  $J/\psi \rightarrow \mu^+\mu^-$  events are taken all over the phase space without any kinematic  
 101 or acceptance requirement, as it can be seen in Fig. 5.

## 102 5. Effect of the offset

We have seen that (9) is a flexible function that can parametrize mass vari-  
 ance distributions if an offset is added to it. Yet, by adding the offset, the  
 marginalization does not yield a generalized hyperbolic distribution for the most  
 general case. We can see that adding an offset to the per-event error distribution

is equivalent to performing a convolution:

$$\begin{aligned}
\int_0^\infty \frac{1}{\sqrt{v}} e^{-\frac{1}{2v}(m-\mu)^2} \rho(v-v_0) dv &= \int_0^\infty \frac{1}{\sqrt{v_0+\Delta}} e^{-\frac{1}{2(v_0+\Delta)}(m-\mu)^2} \rho(\Delta) d\Delta = \\
&= \int_0^\infty \left( \int_{-\infty}^{+\infty} \frac{1}{\sqrt{v_0}} e^{-\frac{1}{2(v_0)}(m-t)^2} \frac{1}{\sqrt{\Delta}} e^{-\frac{1}{2\Delta}(t-\mu)^2} dt \right) \rho(\Delta) d\Delta = \\
&= \int_{-\infty}^{+\infty} \frac{1}{\sqrt{v_0}} e^{-\frac{1}{2(v_0)}(m-t)^2} \left( \int_0^\infty \frac{1}{\sqrt{\Delta}} e^{-\frac{1}{2\Delta}(t-\mu)^2} \rho(\Delta) d\Delta \right) dt = \\
&= \frac{1}{\sqrt{v_0}} e^{-\frac{1}{2(v_0)}(m)^2} * \left( \int_0^\infty \frac{1}{\sqrt{\Delta}} e^{-\frac{1}{2\Delta}(t-\mu)^2} \rho(\Delta) d\Delta \right) \quad (14)
\end{aligned}$$

The convolution of a generalized hyperbolic distribution with a Gaussian is not in general another generalized hyperbolic. However, we can argue that if  $v_0 \gg \Delta$ , we will have a single Gaussian (that is a limit case of the generalized hyperbolic) and, on the contrary, that if  $v_0 \ll \Delta$  in most of the  $\Delta$  range, we will recover the generalized hyperbolic distribution. One can also argue that as we are looking for corrections to the Gaussian distribution, the convolution properties of the Gaussian function still hold approximately. Yet, it will not be exact, and therefore a smeared *Hypatia* distribution:

$$\Upsilon(m, \mu, \sigma^{SR}, \lambda, \zeta, \beta, a, n, v_0) = \frac{1}{\sqrt{v_0}} e^{-\frac{1}{2(v_0)}(m)^2} * I(m, \mu, \sigma^{SR}, \lambda, \zeta, \beta, a, n) \quad (15)$$

103 can provide a better fit than  $I(m, \mu, \sigma, \lambda, \zeta, \beta, a, n)$  for some complicated cases  
104 with high statistics, without a real increase in the number of fit parameters  
105 ( $\sqrt{v_0}$  can be fixed in a somewhat arbitrary point at the start-up of the mass  
106 error distribution), although at the cost of a numerical convolution. The later  
107 can be done in **RooFit** by calling the **RooFFTConvPdf** class on top of the imple-  
108 mentation of  $I(m, \mu, \sigma, \lambda, \zeta, \beta, a, n)$ . If written this way,  $\sqrt{v_0}$  can be interpreted  
109 as an estimate of the mass resolution due to multiple scattering,  $\sigma^{SR}$  the dis-  
110 persion caused by the spatial resolution of the detector given the kinematics of  
111 the final state, and the total resolution would be  $\sigma = \sqrt{v_0 + (\sigma^{SR})^2}$ . Fig. 5  
112 shows a fit of  $I(m, \mu, \sigma, \lambda, \zeta, 0, \infty, 1)$  and  $\Upsilon(m, \mu, \sigma^{SR}, \lambda, \zeta, 0, \infty, 1, 6.5 \text{ MeV}/c^2)$   
113 to the simulated  $J/\psi \rightarrow \mu^+ \mu^-$  data, for the full sample without any kine-  
114 matic constraint, i.e., where very low momentum (MS dominated) and very  
115 high momentum (hit resolution dominated) coexist. The fitting range corre-

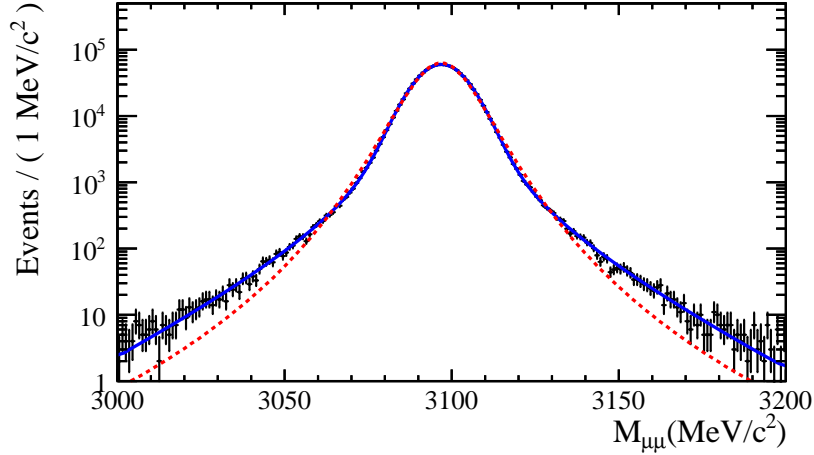


Figure 6: Fit of  $I(m, \mu, \sigma, \lambda, \zeta, 0, \infty, 1)$  (red dashed) and  $\Upsilon(m, \mu, \sigma^{SR}, \lambda, \zeta, 0, \infty, 1, 6.5 \text{ MeV}/c^2)$  (solid blue) to the simulated  $J/\psi \rightarrow \mu^+\mu^-$  data, for the full sample without any kinematic constraint.

116 sponds to about eleven standard deviations. An excellent agreement between  
 117  $\Upsilon(m, \mu, \sigma^{SR}, \lambda, \zeta, 0, \infty, 1, 6.5 \text{ MeV}/c^2)$  and the simulated data is found. We  
 118 failed to find any subsample of the  $J/\psi \rightarrow \mu^+\mu^-$  data that could not be fitted  
 119 by  $\Upsilon(m, \mu, \sigma^{SR}, \lambda, \zeta, 0, \infty, 1, v_0)$ .

## 120 6. Properties of $\lambda$

121 We have seen that using the Hypatia  $\Upsilon$  distribution we can factorize the  
 122 mass resolution modelling into MS and SR. The first part is governed by a  
 123 resolution parameter  $\sigma_0$  that can be estimated from the start-up of the per-  
 124 event variance distribution. The second part is governed by the parameters  
 125  $\zeta, \lambda, \sigma$  of the generalized hyperbolic distribution, where  $\sigma$  corresponds to the  
 126 resolution introduced by SR and where, empirically, we have found that  $\zeta$  is in  
 127 most cases small. In this chapter we will derive a physical meaning for  $\lambda$ , at  
 128 least in the small  $\zeta$  limit.

In the  $\alpha = 0$  ( $\rightarrow \zeta = 0$ ) limit case, the generalized hyperbolic distribution be-  
 comes a *Student's-t* distribution, which can be understood as a marginalization

over a per-event variance density:

$$\rho(v) \propto v^{\lambda-1} e^{-b/v} \tag{16}$$

129 The mean ( $M$ ) and mode ( $\mu$ ) of (16) are:

$$M = \frac{b}{-\lambda - 1}; \mu = \frac{b}{-\lambda + 1} \tag{17}$$

thus

$$\lambda = \frac{1 + M(v)/\mu(v)}{1 - M(v)/\mu(v)} < 0 \tag{18}$$

130 and we can get an estimate of  $\lambda$  by looking at the per-event error (squared)  
 131 distribution, and making the ratio of its mean and mode after shifting it to start  
 132 at zero. But, we can further exploit this relation. From (3) we can suppose that  
 133 the per-event uncertainty will be strongly correlated with the particle momenta.  
 134 Indeed, Fig. 6 supports this.

$$\sigma_i^{SR} \approx c_{te} \times p_{J/\psi, i} \tag{19}$$

135 If this is the case, then  $M(v^{SR})/\mu(v^{SR}) \approx M(p_{J/\psi}^2)/\mu(p_{J/\psi}^2)$  and  $\lambda$  does not  
 136 depend on detector effects, only on particle kinematics. This is an interesting  
 137 result, because if we have a MC simulation with a good description of the  
 138 momentum distribution of the particles in the lab frame, then the values of  $\lambda$   
 139 obtained in simulation should be reasonably valid for data, regardless of having  
 140 an accurate description of detector simulation.

141 **7. Mass constraints on intermediate resonances**

Up to now we have described resolution effects. In more complicated cases, it is sometimes very useful to apply constraints on the decay products. For example, one can significantly improve the invariant mass resolution of  $B_s^0 \rightarrow J/\psi\phi$  by constraining the two muons to have the PDG  $J/\psi$  mass [9]. This kind of approach, although great at improving the overall resolution, can also generate tails on the mass distribution, due to the photon energy radiated in

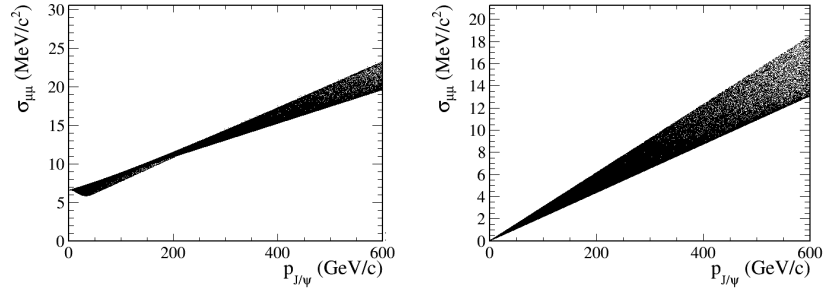


Figure 7: Per-event mass uncertainty versus  $J/\psi$  momentum. Left: with multiple scattering. Right: only detector resolution.

Table 2: Results of a fit to  $\Upsilon(m, \mu, \sigma^{SR}, \lambda, 0, 0, \infty, 1, \sigma^{MS})$  for toy MC  $J/\psi$  events smeared with different values of  $a$  and  $b$  in (3). The parameter  $\sigma^{MS}$  is fixed at the start-up of the per-event variance. The parameter  $\lambda$  is found to be very stable with respect to smearing parameters, which are varied by 100%. However the uncertainty on  $\lambda$  varies significantly, and increases with  $a/b$ .

$a[\times 10^{-3}]$	$b \text{ GeV}/c^{-1}$	$\lambda$	$\sigma^{MS}(\text{MeV}/c^2)$	$\sigma^{SR}(\text{MeV}/c^2)$
3	$2 \times 10^{-5}$	$-2.40 \pm 0.06$	6.81	$4.75 \pm 0.02$
1.5	$2 \times 10^{-5}$	$-2.10 \pm 0.03$	3.53	$3.71 \pm 0.01$
6	$2 \times 10^{-5}$	$-2.67 \pm 0.16$	13.3	$6.3 \pm 0.05$
3	$4 \times 10^{-5}$	$-2.11 \pm 0.03$	7.07	$7.53 \pm 0.03$
3	$1 \times 10^{-5}$	$-2.65 \pm 0.15$	6.67	$3.06 \pm 0.03$

the  $J/\psi \rightarrow \mu^+\mu^-$  decay. Let's consider a simple case in which the constraint is just applied by substituting the mass of the dimuon by the mass of the  $J/\psi$ .

$$m_c^2 = m_{J/\psi}^2 + m_{KK}^2 + 2 \left( \sqrt{m_{J/\psi}^2 + p_{\mu\mu}^2} \sqrt{m_{KK}^2 + p_{KK}^2} - p_{\mu\mu} p_{KK} \cos(\theta) \right) \quad (20)$$

while ideally one would have wanted to implement:

$$m_{true}^2 = m_{J/\psi}^2 + m_{KK}^2 + 2 \left( \sqrt{m_{J/\psi}^2 + p_{J/\psi}^2} \sqrt{m_{KK}^2 + p_{KK}^2} - p_{J/\psi} p_{KK} \cos(\theta) \right) \quad (21)$$

142 The difference  $m_c^2 - m_{true}^2$  is not zero but rather function of the energy  
 143 of the photons generated in the  $J/\psi \rightarrow \mu^+\mu^-$  decay. This difference can be  
 144 greater than zero, generating a tail on the right-hand side. Hence, even with  
 145 a perfect detector resolution, the combination of the mass constraint and the  
 146 photon radiation will generate non-Gaussian tails. In practice, this effect is  
 147 expected to be small because the  $J/\psi \rightarrow \mu^+\mu^-$  decays are selected with a mass  
 148 window cut that allows only low energy photons. Otherwise, it can be partially  
 149 accommodated either by the resolution model (e.g (8)) or by using a CB-like tail  
 150 on the right-hand side (i.e, using a double-sided *Hypatia*). A further discussion  
 151 that goes beyond the scope of this paper is to provide models marginalized over  
 152 per-event errors.

## 153 8. Conclusions

154 We have presented a generalization of the Crystal Ball function that gives  
 155 an excellent description of mass resolution non-Gaussian tails. This function,  
 156 that we name the *Hypatia* distribution,  $I$ , corresponds to a CB-like tail with a  
 157 generalized hyperbolic core. The smeared *Hypatia* distribution,  $\Upsilon$  provides an  
 158 improved description of mass peaks and its fit parameters have clearer funda-  
 159 mental meaning, although the price to pay is a numeric convolution. A second,  
 160 right-hand side CB-like tail can be added in cases where one has other non-  
 161 resolution effects, such as those coming from constraining the mass of interme-  
 162 diate resonances of a decay.

163 **9. Acknowledgments**

164 We would like to thank L. Carson and V. Gligorov for his useful comments  
165 on this draft. We would also like to thank W. Hulsbergen for helpful discussions  
166 during the preparation of this work.

167 **References**

- 168 [1] M. Oreglia, A Study of the Reactions  $\psi' \rightarrow \gamma\gamma\psi$ , Ph.D. thesis (1980).
- 169 [2] J. Gaiser, Charmonium Spectroscopy From Radiative Decays of the  $J/\psi$  and  
170  $\psi'$ , Ph.D. thesis (1982).
- 171 [3] T. Skwarnicki, A study of the radiative cascade transitions between the  
172 Upsilon-prime and Upsilon resonances, Ph.D. thesis, Institute of Nuclear  
173 Physics, Krakow, DESY-F31-86-02 (1986).
- 174 [4] T. Sjöstrand, S. Mrenna, P. Skands, PYTHIA 6.4 physics and manual, JHEP  
175 05 (2006) 026. [arXiv:hep-ph/0603175](https://arxiv.org/abs/hep-ph/0603175), [doi:10.1088/1126-6708/2006/](https://doi.org/10.1088/1126-6708/2006/05/026)  
176 [05/026](https://doi.org/10.1088/1126-6708/2006/05/026).
- 177 [5] A. A. Alves Jr., et al., The LHCb detector at the LHC, JINST 3 (2008)  
178 S08005. [doi:10.1088/1748-0221/3/08/S08005](https://doi.org/10.1088/1748-0221/3/08/S08005).
- 179 [6] R. Aaij, et al., Measurement of  $CP$  violation and the  $B_s^0$  meson decay  
180 width difference with  $B_s^0 \rightarrow J/\psi K^+ K^-$  and  $B_s^0 \rightarrow J/\psi \pi^+ \pi^-$  decays,  
181 Phys.Rev. D87 (2013) 112010. [arXiv:1304.2600](https://arxiv.org/abs/1304.2600), [doi:10.1103/PhysRevD.](https://doi.org/10.1103/PhysRevD.87.112010)  
182 [87.112010](https://doi.org/10.1103/PhysRevD.87.112010).
- 183 [7] L. Amoroso, Recherche intorno alla curve die redditi, Ann. Mat. Pura. Appl.  
184 21 (1925) 123–159.
- 185 [8] A. J. McNeil, R. Frey, P. Embrechts, Quantitative Risk Management Con-  
186 cepts, Techniques and Tools, Princeton University Press.
- 187 [9] J. Beringer, et al., Review of particle physics, Phys. Rev. D86 (2012) 010001.  
188 [doi:10.1103/PhysRevD.86.010001](https://doi.org/10.1103/PhysRevD.86.010001).